PAPER

Check for updates

Microwave-assisted synthesis of glutathione-coated hollow zinc oxide for the removal of heavy metal ions from aqueous systems†

Lateef Ahmad Malik, Arshid Bashir, Taniya Manzoor and Altaf Hussain Pandith (iD) *

Glutathione has tremendous binding potential with metal ions present in water. However, the solubility of glutathione in water limits its productivity in the removal of these toxic ions from aqueous systems. The removability of heavy ions with glutathione and the associated adsorption capability are enhanced; for this purpose, glutathione is coated over hollow zinc oxide particles. Glutathione-coated hollow zinc oxide (Glu@h-ZnO) was successfully synthesized under microwave (MW) conditions using polystyrene (PS) as the template. The as-synthesized material was characterized by Fourier transform infrared (FTIR) spectroscopy, and the results were supported by X-ray diffraction crystallography (XRD), scanning electron microscopy (SEM), transmission electron microscopy (TEM), thermal gravimetric analysis (TGA), differential thermal analysis (DTA), dynamic light scattering (DLS), Brunauer–Emmett–Teller (BET) studies and zeta potential (ζ) analysis. The sorption performance of Glu@h-ZnO towards the uptake of Hg^{2+}, Cd^{2+} and Pb^{2+} ions from an aqueous medium under non-competitive batch conditions was investigated and the material was found to have the maximum affinity for Hg^{2+} ions with a maximum adsorption (q_m) capacity of 233 mg g^{-1}. The adsorption kinetics for Hg^{2+} ions and the effects of pH and ζ on the adsorption properties were also studied in detail. Finally, the experimental data were correlated with theoretical data obtained from density functional theory (DFT) studies and good agreement between the two was obtained.

1. Introduction

Water is indispensable to living creatures on earth; its contamination by toxic heavy metals, such as Hg^{2+}, Pb^{2+}, and Cd^{2+}, is a challenging issue. Among these ions, Hg^{2+} is considered the most dangerous metal ion due to its tendency for biomagnification. Some potent sources of mercury pollution include chloralkali wastewater, oil refineries, power generation plants, paper and pulp manufacturing, rubber processing, and fertilizers industries.[1] From the toxicity point of view, there are three main forms of mercury: inorganic mercury salts, organic mercury compounds and metallic mercury.[2] Inorganic mercury salts, which are water soluble, can cause gut irritation and

severe kidney damage. Organic mercury compounds, which are fat soluble, can cross the blood–brain barrier and cause neurological damage. Mercury metal in vapour form can reach the brain and leads to tremors, depression, and behavioural disturbances. Furthermore, metallic mercury may get bio-transformed into organic mercury by some bacteria and after entering the food chain it could cause a Minamata-like tragedy.[3] Cadmium and lead also have serious toxic effects on living beings. Excessive amounts of cadmium cause kidney damage, renal dysfunction, anaemia, hypertension, *etc.*,[4] while lead poisoning seriously affects the nervous, renal and cardiovascular systems.[5] It is now very important to lower the concentrations of these toxic metal ions to trace levels as they do not have any propensity to be degraded or destroyed.[6] This apprehension has led to stringent regulations regarding acceptable metal concentrations in water.[7] There are many methods that can be employed for the removal of these toxic metal ions. Photo-catalytic reduction of some toxic forms of metal ions, like hexavalent chromium, to a less toxic form is a well-known method reported for waste water treatment.[8,9] Conventional methods, including chemical precipitation, membrane separation, ion exchange, and evaporation, are not desirable because of their low capacities and low removal rates for metals other than Hg^{2+}. Precipitation employing sulfide ions cannot reduce the concentrations of heavy metals below acceptable drinking

Department of Chemistry, University of Kashmir, Hazratbal, Srinagar-190006, Kashmir, India. E-mail: altafpandit23@gmail.com; Fax: +91-194-2414049; Tel: +91-194-2424900; +91-990-6424293

levels.[10] The adsorption method is quite attractive because of its simple design, low cost, swift operability, and high removal efficiency.[11] Various materials, such as zeolites,[12] metal phosphates,[13–15] polymers,[16] biomaterials,[17] layered double hydroxide (LDH)-based materials[18] and sorption resins,[19] have been employed for the adsorption of metal ions. However, nanostructured metal oxides are quite useful in this field as they usually have a large surface area and better removal efficiencies, which make the treatment more economical.[20] ZnO nanoparticles have been employed in this field because of their great biocompatibility, high adsorption capacity, high specific surface area, recyclability, reusability, surface modifiability, and low cost.[21–24] However, the use of nanoparticles in wastewater treatment may cause harmful effects when exposed to the environment owing to flaws in the recovery and disposal issues.[25] Therefore, mechanical supports are used to hold the nanoparticles for possible applications in wastewater treatment. Use of surface modifying agents is an effective way of removing metal ions from water.[26,27] Glutathione, which is a tripeptide, is well-known for its chelation with metal ions in biological systems, which is central to natural detoxification of heavy metals *via* the formation of complexes.[28] Hollow and porous structures[29–32] possess a high specific surface area and, as a result, they find applications in many fields. Such structures possess several different areas of contact, like borders and inner and outer surfaces, which is quite useful for enhanced adsorption properties. The method of synthesis, reaction time and many other factors play a crucial role in determining the size, morphology and composition of the final product.[33] Using MW conditions, reactions can be accelerated and selectivity can be obtained by choosing appropriate MW parameters. It offers advantages like instantaneous and rapid heating, high-temperature homogeneity, selective heating and, in addition, the synthesis and morphology of nanomaterials can be modified in a better way by the efficient and controlled heating provided by MW irradiation.[34]

Here, we report the synthesis of glutathione-coated hollow zinc oxide (Glu@h-ZnO) under microwave conditions using polystyrene as the template. The as-synthesized composite material, after being characterized by various techniques, was used as an adsorbent for the removal of Cd^{2+}, Pb^{2+} and Hg^{2+} ions from an aqueous system. The material was found to possess the highest affinity towards the uptake of Hg^{2+} ion so further adsorption studies, including adsorption isotherms and kinetics, were carried out for this particular ion only. The adsorption of metal ions by Glu@h-ZnO was also tested by theoretical calculations using DFT and good agreement was obtained between DFT and experimental results.

2. Experimental section

2.1 Materials

Styrene (C_8H_8) as the building block of polystyrene (PS), polyvinyl pyrrolidone k-30 (PVP) as a stabilizing agent and sodium persulfate ($Na_2S_2O_8$) as a radical initiator were purchased from Merck and were used without any further purification or processing. Zinc acetate as a source of zinc and reduced

glutathione ($C_{10}H_{17}N_3O_6S$) were purchased from Sigma-Aldrich. In addition, lead nitrate, cadmium nitrate and mercuric chloride, all purchased from Merck, were used to carry out the adsorption studies. Ammonium hydroxide was used for precipitation of zinc ions while ethanol and water were used as the reaction medium.

2.2 Synthesis

2.2.1 Synthesis of polystyrene (PS). Polystyrene was synthesized from styrene by dispersion polymerization method, as already reported in the literature.[35] In this typical synthesis, styrene and PVP in a ratio of 2 : 1 (w/w) were mixed in ethanol under continuous stirring at 343 K. A few drops of sodium persulfate solution were added to polymerize the styrene and the solution was continuously stirred for the next 4 h. The mixture was then centrifuged, washed with ethanol and deionised water many times in order to remove PVP and other impurities, and then dried at 300 K in an oven.

2.2.2 Synthesis of hollow zinc oxide nanoparticles (h-ZnO). To synthesize the hollow zinc oxide nanoparticles, PS was used as the template and an ethanol–water system was used as the reaction medium. An aqueous solution of 10^{-3} M zinc acetate dihydrate and an ethanolic dispersion of PS were mixed together and the mixture was sonicated for 1 hour in an ultrasonic bath, followed by continuous stirring on a magnetic stirrer for the next 2 hours. A few drops of ammonium hydroxide were added as the precipitating agent and the mixture was irradiated by microwaves in a microwave synthesizer (Anton Paar monowave 100) at a temperature of 393 K for 10 minutes. Polystyrene coated with zinc oxide so obtained was centrifuged, washed with ethanol and water, and then calcined in a muffle furnace up to 800 K. During this heating, PS decomposes[36] to CO_2 and H_2O, leaving behind hollow zinc oxide particles.

2.2.3 Synthesis of glutathione-coated hollow zinc oxide (Glu@h-ZnO). Calcination of ZnO at a high temperature eliminates hydroxyl groups that are present on the surface of the ZnO particles,[37] so the calcined ZnO was washed with deionised water to regenerate the surface-bound –OH. Reduced glutathione and h-ZnO particles in a ratio of 1 : 1 (w/w) were mixed together in a limited amount of methanol, as reported in the literature.[38] The mixture was sonicated for more than 1 hour and stirred on magnetic stirrer to ensure complete interaction between the hydroxyl groups of h-ZnO and glutathione to form Glu@h-ZnO. The whole synthetic procedure for Glu@h-ZnO is shown in Scheme 1.

2.3 Characterization

Fourier transform infrared (FTIR) spectra of the samples were recorded over the range of 400–4000 cm^{-1} using a Bruker (Alpha 200486) FTIR spectrometer. The crystalline structure of the prepared samples was characterized by X-ray diffractometer (Ultima-IV, Rigaku Corporation, Tokyo, Japan) using Cu Kα radiation. The microscopic analysis was carried out using a scanning electron microscope (Hitachi, S3000H. Japan) and a transmission electron microscope (JEM-100 CX II). Thermal
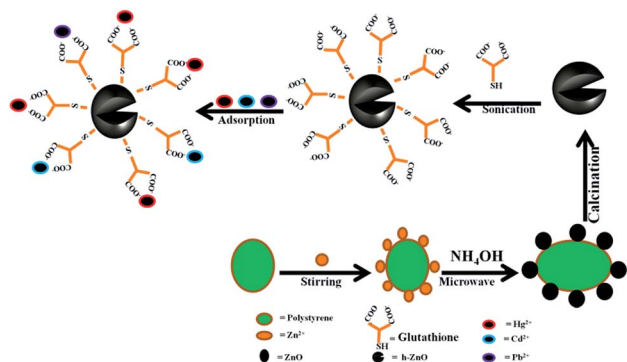
Scheme 1 Schematic representation of the synthesis of Glu@h-ZnO and its use as an adsorbent for heavy metal ions.

analysis (TGA/DTA) was carried out using a Simultaneous Thermal Analyzer (STA, Linseis, USA 6807/8835/16). An accurately weighed sample was placed in an alumina crucible and heated from room temperature to 973 K at a heating rate of 283 K min^{-1}. The size distributions and zeta potential (ζ) of the particles were determined with an Anton Paar Litesizer 500 by the DLS technique. Before DLS was carried out, each sample was sonicated for 10 minutes to obtain a fine suspension of the samples for better results. The surface area of the samples was measured by nitrogen adsorption–desorption isotherms using the Brunauer–Emmett–Teller (BET; Micromeritics ASAP 2020) method.

2.4 Adsorption studies

The batch adsorption experiments were carried out with 0.020 g of composite material and 20 ml of 30 ppm aqueous solutions of Hg^{2+}, Cd^{2+}, and Pb^{2+} at room temperature and neutral pH. The suspensions were shaken for 6 h to achieve adsorption equilibration. The suspensions were filtered and the concentrations of the metal ions in the filtrate were determined using an atomic absorption spectrometer (PerkinElmer, AAnalyst 800). The adsorption percentage of metal ions on the composite material was calculated using eqn (1).

$$\text{Adsorption percentage} = \left(\frac{C_0 - C_e}{C_0} \right) \times 100 \quad (1)$$

The affinity of Glu@h-ZnO towards the metal ions can also be expressed in terms of the distribution coefficient (K_d), calculated by using eqn (2), and the equilibrium adsorption capacity (q_e) of the material for a particular ion is obtained using eqn (3).

$$K_d = (C_0 - C_e/C_e) \frac{V}{m} \ \left(\text{mL g}^{-1}\right) \quad (2)$$

$$q_e = 10^{-3} \times (C_0 - C_e) \times \frac{V}{m} \ \left(\text{mg g}^{-1}\right) \quad (3)$$

where V is the volume of the metal ion solution (in ml), C_0 is the initial concentration of metal ions, C_e is the concentration of metal ions after adsorption when equilibrium is attained and m is the mass of the adsorbent (in g).

2.5 Kinetic studies

Kinetic studies were carried out for Hg^{2+} at 298 K with various adsorption contact times (10–280 min). For each operation, 0.020 g of solid sample was taken into a 50 ml flask containing 20 ml of 30 ppm aqueous solution of Hg^{2+}. At specified time intervals, the suspensions were centrifuged and the ion concentration left in the solution phase after adsorption was determined by AAS.

2.6 Computational studies

To study the interaction between the composite material and metal ions, *viz.*, Cd^{2+}, Pb^{2+}, and Hg^{2+}, the Glu@h-ZnO–metal ion complexes were optimized by density functional theory (DFT) using LanL2DZ and B3LYP as the basis set and functional, respectively. A single point energy (SPE) scan was carried out in order to give a comparative account of the interactions between the composite and the corresponding metal ions, which was expressed in terms of interaction energy, as calculated using eqn (4):

$$\Delta E = [E_{\text{Glu@h-ZnO}} + E_{\text{metal ion}}] - E_{\text{Glu@h-ZnO–metal ion}} \ (\text{kJ mol}^{-1}) \quad (4)$$

where $E_{\text{Glu@h-ZnO}}$, $E_{\text{metal ion}}$ and $E_{\text{Glu@h-ZnO–metal ion}}$ are the energy of the composite material, metal ion and composite material–metal ion complex, respectively.

3. Results and discussion

3.1 FTIR analysis

FTIR spectra of reduced glutathione, h-ZnO and Glu@h-ZnO were recorded in order to confirm the purity of these materials. There are two types of OH bands present in the FTIR spectrum for ZnO, one corresponding to –OH groups attached to the metal ions and the other attached to the surfaces.[32] In the FTIR spectrum of h-ZnO (Fig. 1), the peaks at around 511 cm^{-1}, 1130 cm^{-1}, and 3440 cm^{-1} are attributed to Zn–O deformation, ZnO stretching, and O–H stretching, respectively. The two other prominent peaks at around 1460 cm^{-1} and 1630 cm^{-1} in the case of ZnO and the composite material are due to O–H groups attached to metal ions and to the surfaces.[39,40]
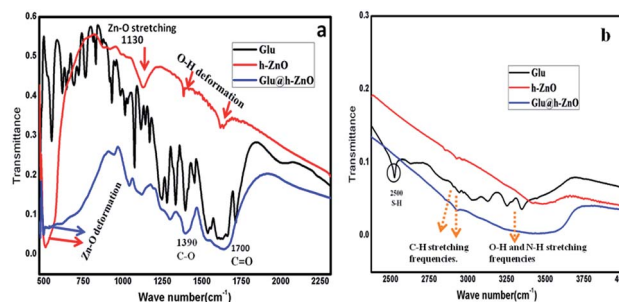

Fig. 1 FTIR spectra of glutathione-coated hollow zinc oxide, reduced glutathione and hollow zinc oxide in the frequency range of 450 cm^{-1} to 2350 cm^{-1} (a) and from 2350 cm^{-1} to 4000 cm^{-1} (b).

The IR band at around 1700 cm^{-1} corresponding to the $>$C$=$O stretching frequency in addition to the other characteristic bands of the –COOH group at around 1300 cm^{-1} and 1400 cm^{-1} are present in the FTIR spectra of both glutathione and Glu@h-ZnO. Besides, in both of these materials, IR bands at around 2800 cm^{-1} and 2900 cm^{-1} are present, which are attributed to the methyl stretching frequencies. The presence of such characteristic peaks of glutathione in the composite material suggests a possible coating of glutathione over the hollow ZnO surface. Furthermore, a prominent IR band at around 2500 cm^{-1}, corresponding to S–H deformation, is present in the reduced glutathione but not in the Glu@h-ZnO spectrum. The diminishing of the S–H peak may be because glutathione binds to h-ZnO through sulfur, as a result of which the existence of an S–H bond in the composite is highly unlikely.

3.2 Thermal gravimetric (TGA) analysis

Thermal analysis, in terms of TGA and DTA, was carried out for the composite material as well as for the individual components for comparison purposes (Fig. 2). In the case of pure ZnO, weight loss occurs up to 200 °C and thereafter it remains constant. This weight loss is attributed to the removal of surface-bound water and the decomposition of Zn(OH)$_2$.[41,42] Contrary to this, an extra weight loss stage is observed in case of Glu@h-ZnO in the temperature range of 270–580 °C, which is attributed to the decomposition of glutathione. It is important to note that pure glutathione starts to decompose at around 200 °C, as can be seen from its thermogram. Delayed decomposition of glutathione in the case of Glu@h-ZnO indicates that its thermal stability is enhanced after it is coated over the ZnO surface. The same thing is also reflected by the DTA results. Endothermic peaks at around 100 °C in the case of ZnO and Glu@h-ZnO indicate the loss of water. Another endothermic peak at 270 °C in the case of Glu@h-ZnO represents the melting of glutathione. However, the same peak in the case of pure glutathione appears at 200 °C, which indicates a substantial improvement in the thermal stability of Glu@h-ZnO. Exothermic peaks in the temperature range of 380–450 °C for pure glutathione and Glu@h-ZnO represent oxidation of glutathione. Exothermic peaks in the temperature range of 470–

530 °C for ZnO and Glu@h-ZnO may be attributed to crystallization of the amorphous part of ZnO.[43]

Further, from the TGA curve of Glu@h-ZnO, it can be inferred that there is approximately 50% weight loss due to glutathione. The value is close to the 1 : 1 ratio of h-ZnO and glutathione taken at the time of its synthesis.

3.3 Microscopic studies

The SEM images of h-ZnO (Fig. 3a–d) clearly show that ZnO particles are hollow and some big cavities are visible in the SEM images at higher magnification. Furthermore, the surface of the uncoated hollow particles appears to be smooth with very little agglomeration of particles. On the other hand, the Glu@h-ZnO composite material appears as agglomerated and the hollowness of the particles is not quite visible in the SEM images (Fig. 3e and f). Agglomeration and diminishing of the hollow character in the case of Glu@h-ZnO may be due to the extensive coating of glutathione over the hollow ZnO particles.

Fig. 4 shows the TEM images of hollow ZnO and Glu@h-ZnO at different magnifications. The surface of the uncoated hollow ZnO (Fig. 4a and b) appears to be smoother in the TEM images compared to the surface of the coated particles (Fig. 4c–f). From TEM analysis, the average size of the Glu@h-ZnO particles is around 35 nm. A glutathione coating of approximately 11 nm thickness can be seen over the surface of a h-ZnO particle (inset Fig. 4f). The glutathione coating has a drastic effect in screening the hollow character of the ZnO particles as the cavities are occupied by glutathione molecules as well. As a result, the hollowness of the particles is not quite visible in the TEM images. The diameter of the cavity is not uniform and varies from particle to particle. The biggest cavity is about 34 nm in diameter.

3.4 XRD analysis

Fig. 5 shows the XRD pattern for the uncoated h-ZnO and Glu@h-ZnO. It can be seen that the peak intensity in the XRD pattern of h-ZnO is sharp and narrow, confirming that the sample is of high quality with good crystallinity. The lines at 2θ values equal to 31.76°, 34.58°, and 36.67° are due to reflection from the crystallographic (100), (002), and (101) planes, respectively, while the peaks at 47.9°, 57.02°, 63.3°, 66.68°,
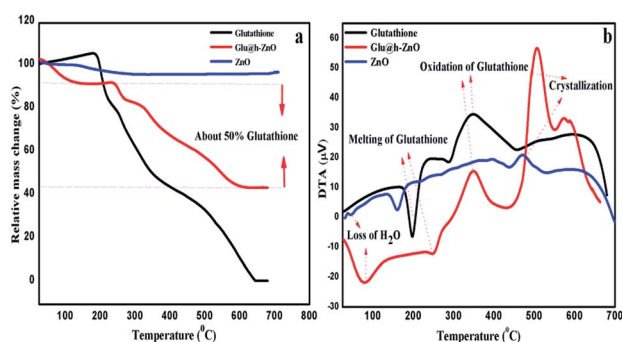

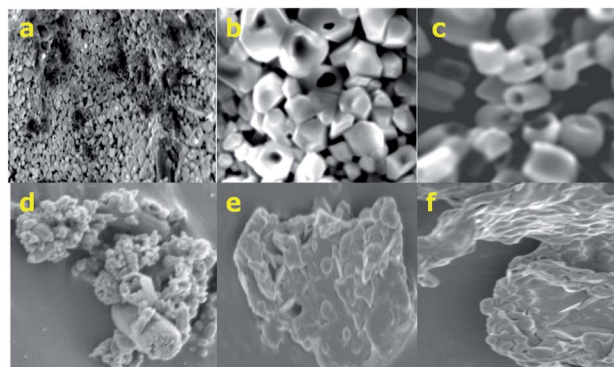Fig. 2 TGA (a) and DTA (b) curves of h-ZnO, glutathione and Glu@h-ZnO.

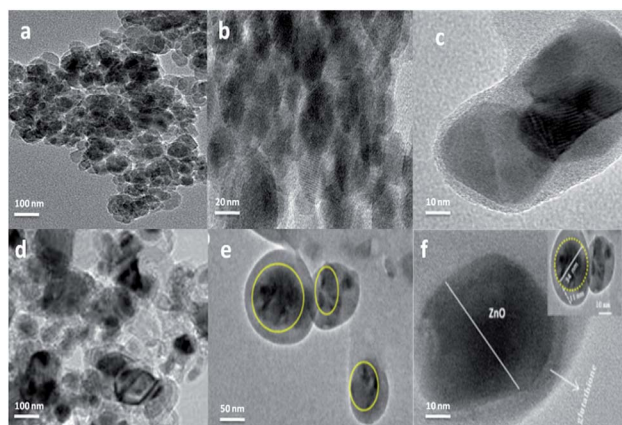Fig. 3 SEM images of h-ZnO (a–d) and Glu@h-ZnO (e and f).

Fig. 4 TEM images of hollow ZnO (a and b) and Glu@h-ZnO (c–f).

68.26° and 69.36° correspond to the 102, 110, 103, 200, 112 and 201 planes, respectively, and they are in accordance with the wurtzite structure of ZnO (International Centre for Diffraction Data, JCPDS 5-0664). No impurity peaks were observed, suggesting that high-purity ZnO was obtained. The XRD pattern of Glu@h-ZnO has similar peaks except the peak intensity is reduced and the low intensity peak corresponding to the (200) plane is absent in the composite when compared with pure h-ZnO. The reduction in the peak intensity[44] and the absence of the peak pertaining to the 200 plane indicate the successful coating of glutathione over the h-ZnO particles. The peak intensity is sharp, even in the composite, which may be due to the high crystallinity acquired as the outcome of the calcination during the formation of the h-ZnO.

3.5 DLS measurements

3.5.1 Particle size and zeta potential (ζ). Particle size distribution by intensity was obtained for both h-ZnO and Glu@h-ZnO. The particle size measurements for Glu@h-ZnO at pH 7 show that it has a hydrodynamic diameter of 1483.50 nm and PDI of 17.3%. The PDI value of greater than 10% indicates the heterogeneous nature of particles, which may be attributed to the non-uniform coating of glutathione over the h-ZnO particles owing to different sized cavities in the h-ZnO. The effect of pH on the hydrodynamic diameter of the Glu@h-ZnO particles was also determined (Fig. S1a†). It was found that
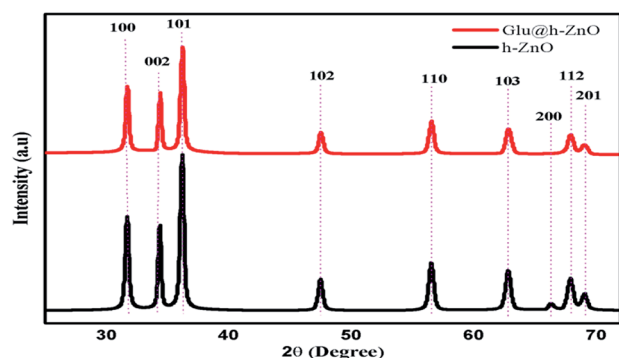
the hydrodynamic diameter showed a continuous decrease when the pH was increased from 4 to 8. This is because, even at pH 4, the surface of Glu@h-ZnO is sufficiently negative and when the pH is increased, more and more –COOH groups of glutathione are de-protonated, making the surface more negatively charged (as revealed from the zeta potential studies). The higher the magnitude of the charge on the surface, the more strongly they will repel, thus preventing the possibility of agglomeration.[45] On the other hand, a hydrodynamic diameter of 8197 nm at neutral pH was obtained for h-ZnO from DLS studies (Fig. S1b†) with a polydispersity index (PDI) of 9.7% (less than 10%) indicating the monodispersed nature of the material.

Zeta potential measurements were carried out for both Glu@h-ZnO and uncoated h-ZnO (Fig. S2†). The ζ of uncoated h-ZnO was found to be only -3.1 mV at neutral pH, which is very small compared to the ζ(-21.72 mV) of Glu@h-ZnO under the same conditions. The effect of pH on the ζ was also determined for Glu@h-ZnO. It can be seen that at pH 4, the ζ of Glu@h-ZnO is -6.72, which may be due to some surface-bound –OH groups and glutathione molecules remaining de-protonated even at pH 4. When the pH is increased from 4 to 8, more and more –COOH groups of glutathione and surface-bound –OH groups are de-protonated, making the surface more negative. The variation of the ζ and hydrodynamic diameter of Glu@h-ZnO with pH is summarized in Table 1 and it can be seen that there is an inverse relationship between surface charge and hydrodynamic diameter.

3.6 BET studies

The surface area of the material plays a large role in the process of adsorption of metal ions. The higher the surface area, the more sites will be available for the metal ions for adsorption to take place. In this regard, we evaluated the surface area of both hollow ZnO and Glu@h-ZnO using the nitrogen adsorption–desorption method at 77 K. The N_2 adsorption–desorption isotherms in the relative pressure range of 0 to 1 are shown in Fig. 6. The surface areas calculated for hollow ZnO and Glu@h-ZnO using BET isotherms were found to be 17.1 $m^2\,g^{-1}$ and 12.3 $m^2\,g^{-1}$, respectively. The BET surface area calculated for hollow ZnO is much higher when it is compared to the normal ZnO.[46] This indicates that glutathione coating over hollow ZnO will have a prominent effect in promoting the adsorption capability of Glu@h-ZnO towards heavy metal ions. Furthermore, when the surface area of uncoated and coated hollow ZnO was compared, a significant decrease was observed in the case of the latter. This decrease in surface area may be attributed to the occupation of cavities by glutathione molecules during the process of coating.

3.7 Adsorption studies

3.7.1 Heavy metal removal. The glutathione molecules present on the surface of the h-ZnO have a good tendency to bind with the metal ions, so the metal ion removal characteristics of Glu@h-ZnO were investigated by carrying out adsorption experiments with individual solutions of Pb^{2+}, Cd^{2+}, and Hg^{2+}, as shown in Table 2.

Fig. 5 XRD patterns of Glu@h-ZnO and h-ZnO.

Table 1 Variation of ζ and the hydrodynamic diameter of Glu@h-ZnO particles with pH

pH	4	5	6	7	8
Zeta potential (mV)	−6.72	−10.55	−13.62	−21.72	−23.39
Hydrodynamic diameter (nm)	2626	1823	1483	1186	881
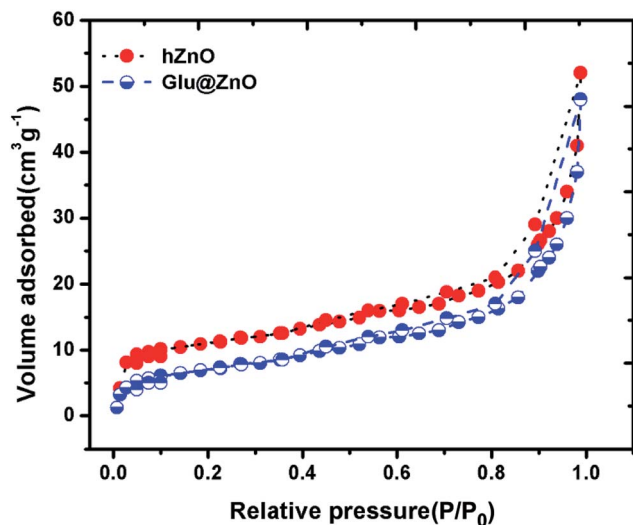
Fig. 6 Nitrogen adsorption–desorption isotherms of hollow ZnO and the Glu@h-ZnO composite recorded at 77 K.

It can be seen from the table that the concentrations of these ions decrease from the starting value of ∼30 ppm and the maximum decrease was obtained in the case of Hg^{2+}, indicating that the adsorption ability of Glu@h-ZnO towards Hg^{2+} is higher than those for Cd^{2+} and Pb^{2+} ions.
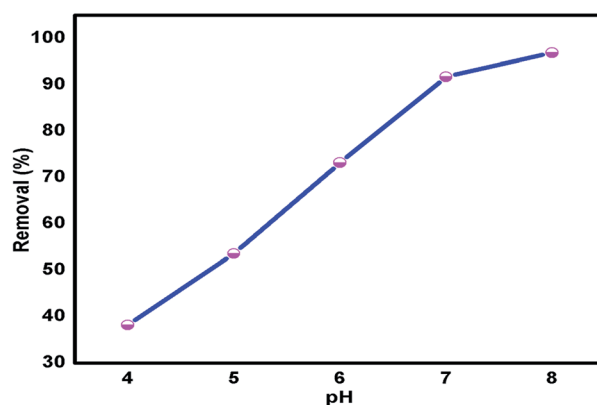
The affinity of Glu@h-ZnO towards the uptake of these metal ions follows the order: $Hg^{2+} > Cd^{2+} > Pb^{2+}$, as shown in Fig. S3,† which is the same as previously reported by our group[47] and is also in good agreement with the data obtained from the present DFT studies. As the material shows the highest affinity towards the uptake of Hg^{2+} ions, this ion was selected for further studies.

3.7.2 Effect of pH on adsorption. Metal ions in aqueous solution can be present in various forms at different pH values. Therefore, the pH of the solution plays an important role in the adsorption of metal ions on Glu@h-ZnO. The adsorption of metal ions on Glu@h-ZnO was investigated at pH values from 4

to 8. As shown in Fig. 7, the adsorption of Hg^{2+} increases continuously as the pH increases from 4 to 8.

At pH 4 only about 40% of Hg^{2+} is removed, but the removal reaches about 97% at a pH of 8. The mode of interaction is expected to be electrostatic[48] between the metal ions and $-COO^-$ groups of Glu@h-ZnO and the same is revealed from the present DFT studies and pH experiments. The surface charge of Glu@h-ZnO is negative in the pH range of 4 to 8 with a higher magnitude at higher pH values, as revealed from DLS studies. This means that a pH higher than 4 is beneficial for the ionization of the oxygen-containing functional groups on the surface of Glu@h-ZnO, which play a significant role in the uptake of metal ions. The negative charges generated on the Glu@h-ZnO surface enhance the adsorption capacity of Glu@h-ZnO and, simultaneously, the electrostatic attraction becomes more important. The adsorption of metal ions decreases at lower pH values owing to the low dissociation of the functional groups and competition between H^+ ions and metal ions for the same sorption sites. Although there is greater adsorption of metal ions at higher pH values, we carried out further studies at neutral pH because at basic pH most of the metal ions are precipitated and also because the pH of the aqueous systems happens to be around 7.

3.7.3 Batch adsorption studies for Hg^{2+} ion uptake. From the results described above, Glu@h-ZnO shows the highest selectivity for the removal of Hg^{2+}. The maximum adsorption capacity of the material was determined from an adsorption equilibrium study. The Hg^{2+} uptake by Glu@h-ZnO was found to increase successively with increasing concentration (10–600 ppm) of Hg^{2+} ions, as shown in Table 3.

Table 2 Percentage removal and K_d values of Pb^{2+}, Cd^{2+}, and Hg^{2+} ions by Glu@h-ZnO at pH = 7, T = 298 K, m = 0.02 g, V = 20 ml, conc. of metal ion = ∼30 ppm and contact time = 6 h

Metal ion	C_0 (ppm)	C_e (ppm)	Metal ion removal (%)	K_d (ml g^{-1})
Pb^{2+}	29.75	4.97	83.29	9.8×10^3
Cd^{2+}	30.15	4.05	86.57	1.3×10^4
Hg^{2+}	29.36	1.12	96.18	5.0×10^4

Fig. 7 Variation of Hg^{2+} ion adsorption by Glu@h-ZnO at various pH values at T = 298 K, mass of adsorbent (m) = 0.020 g and volume of metal ion solution (V) = 20 ml.

The percent ion removal, q_e and K_d values over this wide range of initial concentration (10–600 ppm) of metal ion were obtained using eqn (1), (2) and (3), respectively. The maximum adsorption capacity (q_m) of Glu@h-ZnO for Hg^{2+} was found to be around 233 mg g^{-1} (Fig. 8a), beyond which no appreciable change in the q_e value was found.

This q_m value for Glu@h-ZnO is quite satisfactory when compared to the q_m values of other materials reported in the literature (Table 4). To correlate the amount of Hg^{2+} ions adsorbed by unit mass of adsorbent, the Langmuir adsorption isotherm[49] was used. In this model, the adsorbate moieties (Hg^{2+} ions) are assumed to undergo monolayer type coverage over energetically identical adsorption sites of the adsorbent surface. This model assumes that no further adsorption can take place at a site that is already occupied by the adsorbate moiety. The Langmuir isotherm model can be written as shown in eqn (5):

$$\frac{1}{q_e} = \frac{1}{q_m} + \frac{1}{bq_mC_e} \quad (5)$$

where q (mg g^{-1}) represents the equilibrium adsorption capacity of Hg^{2+} ions adsorbed, C_e (mg L^{-1}) is the Hg^{2+} ion concentration at equilibrium, q_m (mg g^{-1}) is the theoretical maximum adsorption capacity and b is the Langmuir constant. The values of q_m and b were obtained from the intercept and the slope of the linear plot of $1/q_e$ vs. $1/C_e$ (Fig. 8b), respectively. The theoretical maximum adsorption capacity ($q_{m,cal}$) was found to be 222.22 mg g^{-1}, which is very close to the experimental maximum adsorption capacity ($q_{m,exp}$ = 233 mg g^{-1}) given in Table 5.

Furthermore, the correlation coefficient being close to 1 (R^2 = 0.9888) suggests the adsorption of Hg^{2+} ions on the surface of Glu@h-ZnO is monolayer and can be well described by the Langmuir model. The separation factor (R_L) was evaluated by using eqn (6) to determine whether the adsorption process is linear ($R_L = 1$), unfavourable ($R_L > 1$), favourable ($0 < R_L < 1$) or irreversible ($R_L = 0$).[58] In our case, the value of R_L was 0.225, indicating the favourable adsorption of Hg^{2+} on Glu@h-ZnO.

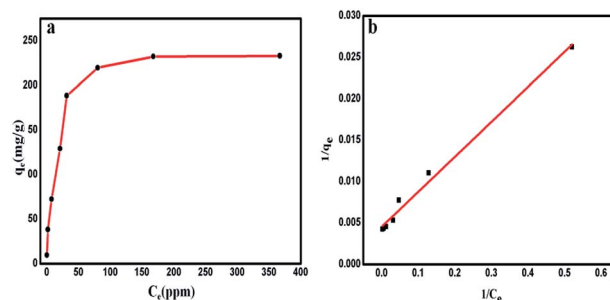$$R_L = \frac{1}{1 + bC_0} \quad (6)$$

Fig. 8 Variation of the equilibrium adsorption capacity (q_e) of Glu@h-ZnO towards the uptake of Hg^{2+} solutions of different concentrations (10–600 ppm) at pH = 7 and T = 298 K (a). The Langmuir adsorption isotherm model for the adsorption of Hg^{2+} ions on Glu@h-ZnO (b).

where C_0 is the lowest initial concentration of metal ions and b is the Langmuir adsorption constant.

3.7.4 Adsorption kinetics. It is very significant to investigate the adsorption kinetics in order to study the adsorption rate and pathways of adsorption until equilibrium is reached. Adsorption kinetic experiments for Hg^{2+} at various adsorption contact times (5–280 min) were performed and it can be seen from Fig. 9A that the rate of adsorption is very fast in the first 40–50 minutes but thereafter it slows down and equilibrium is attained after a contact time of 100 minutes. The rate of adsorption was determined by using two different rate equations, pseudo-first order and pseudo-second order, and a comparison was drawn between the experimental and calculated data, as shown in Table 6. The two kinetic rate equations can be written as follows.[59]

Pseudo-first order

$$\ln(q_e - q_t) = \ln q_e - k_1t \quad (7)$$

Table 4 A comparison of the adsorption capacities of various adsorbents for Hg^{2+} ions

S. no	Adsorbent	q_m (mg g^{-1})	Ref.
1	GAC[a]	20.83	50
2	MNPs-DTC[b]	47.87	51
3	CSTG[c]	98	52
4	PANI–PS[d] composite	148	53
5	Mercaptosuccinic acid–LDH[e]	161	54
6	PAM/ATP[f]	192	55
7	Glu@h-ZnO[g]	233	Current work
8	KMS-2[h]	297	56
9	KMS-1[i]	377	57
10	MoS$_4$–LDH[j]	500	18

[a] Carboxymethylated granular activated carbon (GAC). [b] Magnetic nanoparticles (MNPs) of Fe_3O_4 functionalized by dithiocarbamate (DTC). [c] Chitosan-thioglyceraldehyde Schiff's base cross-linked magnetic resin (CSTG). [d] Polyaniline–polystyrene composite (PANI–PS). [e] Mercaptocarboxylic acid intercalated Mg–Al layered double hydroxide. [f] Polyacrylamide/attapulgite (PAM/ATP). [g] Glutathione-coated hollow ZnO (Glu@h-ZnO). [h] Layered $K_2MgSn_2S_6$ (KMS-2). [i] Layered metal sulfides (KMS-1). [j] Layered double hydroxide intercalated with the MoS_4^{2-} ion.

Table 3 Removal percentage, adsorption capacity (q) and distribution coefficient (K_d) value of Glu@h-ZnO towards the uptake of different Hg^{2+} ion concentrations at pH = 7, T = 298 K, m = 0.02 g, V = 20 ml, V/m = 1000 ml g^{-1} and contact time = 6 h

C_0 (ppm) (approx.)	C_e (ppm)	Removal (%)	q_e (mg g^{-1})	K_d (ml g^{-1})
10	0.31	96.9	9.69	3.1×10^4
40	1.92	95.2	38.08	2.0×10^4
80	7.74	90.32	72.26	9.3×10^3
150	20.97	86.02	129.03	6.2×10^3
220	31.44	85.71	188.56	6.0×10^3
300	80.35	73.21	219.65	2.7×10^3
400	167.80	58.05	232.2	1.4×10^3
600	366.98	38.83	233.02	6.3×10^2

Table 5 Adsorption isotherm constants for the adsorption of Hg^{2+} by Glu@h-ZnO at $T = 298$ K

$q_{m,cal}$ (mg g^{-1})	b (L mg^{-1})	R^2	R_L
222.22	0.34	0.9888	0.225
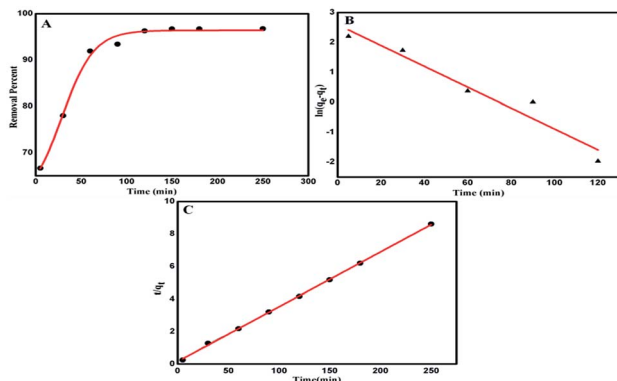
Fig. 9 Removal percentage of Hg^{2+} as a function of time (A). Pseudo-first order kinetic plot for Hg^{2+} ion removal (B) and pseudo-second-order kinetic plot for Hg^{2+} ion removal (C).

Pseudo-second order

$$\frac{t}{q_t} = \frac{1}{k_2 q_e^2} + \frac{t}{q_e} \qquad (8)$$

where q_e (mg g^{-1}) and q_t (mg g^{-1}) are the amounts of Hg^{2+} adsorbed at equilibrium and at time t, respectively, while k_1 (min^{-1}) and k_2 (g mg^{-1} min^{-1}) are the equilibrium rate constants of the pseudo-first-order and pseudo-second-order rate equations, respectively.

The value of k_1 was obtained from the slope of the plot of $\ln(q_e - q_t)$ vs. t (Fig. 9B) while k_2 was obtained from the intercept of the plot of t/q_t vs. t (Fig. 9C). The various pseudo-first-order and pseudo second order kinetic parameters are summarized in Table 6. The correlation coefficient (R^2) corresponding to the pseudo first order model is only 0.9333 but the value is much closer to 1 (being equal to 0.9995) for the pseudo second order rate model. Furthermore, it can be seen that the $q_{e,cal}$ value is much close to the $q_{e,exp}$ value for the pseudo-second order model while the two differ marginally for the pseudo-first order model. These results indicate that a pseudo-second order kinetic model is suitable for describing the adsorption of Hg^{2+} ions on Glu@h-ZnO particles where chemical forces are holding the metal ions and the adsorbent together.[60]

3.8 Computational studies

To study the interaction between Glu@h-ZnO and metal ions, viz., Cd^{2+}, Pb^{2+}, and Hg^{2+}, density functional theory studies were carried out using the LanL2DZ basis set at the B3LYP level of theory. From these theoretical calculations, the optimized geometries and interaction energies of the composite–metal ion systems were obtained. The optimized geometries are given in Fig. 10 and from these computational studies it was found that the most favourable metal ion interaction takes place with the oxygen of the glutathione molecule.

SPE scans were carried out for all the complex models in order to give a comparative account of the interaction for all the complex models studied, as shown in Fig. S4.† The interaction between the composite and the corresponding metal ions was expressed in terms of interaction energy (in kJ mol^{-1}) and was found to be −2218.29 for Pb^{2+}, −2443.34 for Cd^{2+} and −2500.46 for Hg^{2+}. This indicates that Glu@h-ZnO has the highest affinity for Hg^{2+}, followed by Cd^{2+} and then Pb^{2+} ions. The computational results are in good congruence with the experimental values obtained from the adsorption studies of the composite material.

3.9 Proposed mechanism of adsorption

Metal ion binding to Glu@h-ZnO is preferentially based on electrostatic interactions between the negatively charged groups on Glu@h-ZnO and the positively charged metal ions. Investigation of the effect of pH on adsorption revealed very low adsorption at low pH values, mainly because of the diminishing negative charge on the Glu@h-ZnO surface at lower pH values, as a result of which the ionic interactions become weaker and the adsorption of metal ions is slowed down in acidic medium. The DFT studies also suggested that electrostatic interactions
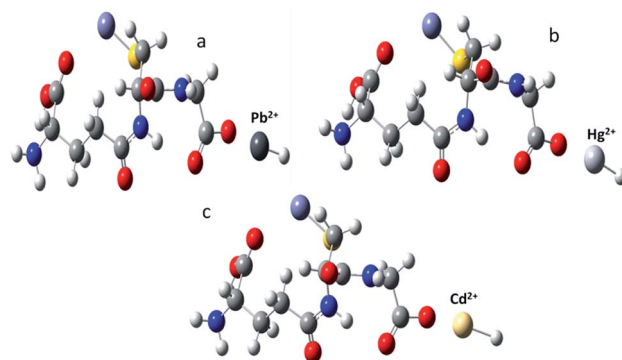
Fig. 10 Optimized geometries of metal ion complexed glutathione obtained from DFT studies: (a) Pb^{2+}; (b) Hg^{2+}; and (c) Cd^{2+}.

Table 6 Kinetic parameters obtained for the adsorption of Hg^{2+} ions by Glu@h-ZnO

Initial concentration	Pseudo-first order				Pseudo-second order			
	k_1 (min^{-1})	R^2	$q_{e,exp}$	$q_{e,cal}$	k_2 (g mg^{-1} min^{-1})	R^2	$q_{e,exp}$	$q_{e,cal}$
30 ppm	3.48×10^{-2}	0.9333	29.02	13.35	7.28×10^{-3}	0.9995	29.02	29.70

are mainly responsible for the adsorption of metal ions on Glu@h-ZnO. From the DFT studies, it was found that the oxygen atoms of the –COOH group have more interacting power than the nitrogen atoms present in the glutathione moiety. Computational results for adsorption of metal ions by Glu@h-ZnO indicate the transfer of hydrogen from the –COOH of glutathione to the metal ion (Fig. 10) for optimized electrostatic interactions between the two. The transfer of H$^+$ from the –COOH group to the metal ion certainly enhances the negative and positive charges on the glutathione and metal ion, respectively, for stronger ionic bonding during adsorption. From this discussion, it can be concluded that pure ionic interactions are responsible for holding the metal ions on Glu@h-ZnO during the process of adsorption.

4. Conclusions

Glu@h-ZnO was successfully synthesized under microwave conditions, as confirmed by various characterization techniques. The as-synthesized material was used as an adsorbent for the uptake of Hg^{2+}, Cd^{2+}, and Pb^{2+} ions and the maximum uptake was found towards Hg^{2+} ions, with a maximum adsorption capacity of 233 mg g^{-1}, which is reasonably good for this material. The adsorption of Hg^{2+} by Glu@h-ZnO follows pseudo-second-order rate kinetics and can be well described by the Langmuir model. Finally, DFT studies were carried out to correlate theoretical results with the experimental data. The computational results so obtained were in good congruence with the experimental values obtained from adsorption studies using the composite material.

Conflicts of interest

There are no conflicts to declare.

Acknowledgements

References

1 B. J. Kim, K. M. Bae, K. H. An and S. J. Park, *Bull. Korean Chem. Soc.*, 2011, **32**, 1321–1326.

2 N. J. Langford and R. E. Ferner, *J. Hum. Hypertens.*, 1999, **13**, 651–656.

3 T. Wajima and K. Sugawara, *Fuel Process. Technol.*, 2011, **92**, 1322–1327.

4 A. Bashir, S. Ahad and A. H. Pandith, *Ind. Eng. Chem. Res.*, 2016, **55**, 4820–4829.

5 G. Flora, D. Gupta and A. Tiwari, *Interdiscip. Toxicol.*, 2012, **5**, 47–58.

6 M. Dinari, R. Soltani and G. Mohammadnezhad, *J. Chem. Eng. Data*, 2017, **62**, 2316–2329.

7 A. S. Adeleye and A. A. Keller, *Water Res.*, 2014, **49**, 236–250.

8 E. Hu, X. Gao, A. Etogo, Y. Xie, Y. Zhong and Y. Hu, *J. Alloys Compd.*, 2014, **611**, 335–340.

9 S. Wang, J. Li, X. Zhou, C. Zheng, J. Ning, Y. Zhonga and Y. Hu, *J. Mater. Chem. A*, 2014, **2**, 19815–19821.

10 D. R. Tonini, D. A. Gauvin, R. W. Soffel and W. P. Freeman, *Environ. Prog.*, 2003, **22**, 167–173.

11 X. H. Wang, W. Y. Deng, Y. Y. Xie and C. Y. Wang, *Chem. Eng. J.*, 2013, **228**, 232–242.

12 G. Blanchard, M. Maunaye and G. Martin, *Water Res.*, 1984, **18**, 1501–1507.

13 K. G. Varshney, A. H. Pandith and U. Gupta, *Langmuir*, 1998, **14**, 7353–7358.

14 K. G. Varshney and A. H. Pandith, *Langmuir*, 1999, **15**, 7422–7425.

15 K. G. Varshney and A. H. Pandith, *J. Indian Chem. Soc.*, 2001, **78**, 250–253.

16 J. S. Liu, Y. Ma, T. W. Xu and G. Q. Shao, *J. Hazard. Mater.*, 2010, **178**, 1021–1029.

17 A. B. Albadarin, A. H. Al-Muhtaseb, N. A. Al-laqtah, G. M. Walker, S. J. Allen and M. N. M. Ahmad, *Chem. Eng. J.*, 2011, **169**, 20–30.

18 L. Ma, Q. Wang, S. M. Islam, Y. Liu, S. Ma and M. G. Kanatzidis, *J. Am. Chem. Soc.*, 2016, **138**, 2858–2866.

19 V. Tharanitharan and K. Srinivasan, *Asian J. Chem.*, 2010, **22**, 3036–3046.

20 H. Qian, Y. Hu, Y. Liu, M. Zhou and C. Guo, *Mater. Lett.*, 2012, **68**, 174–177.

21 A. Ali, H. Zafar, M. Zia, I. u. Haq, A. R. Phull, J. S. Ali and A. Hussain, *Nanotechnol., Sci. Appl.*, 2016, **9**, 49–67.

22 S. Chaudhary, A. Umar, K. K. Bhasin and S. Baskoutas, *Materials*, 2018, **11**, 287, DOI: 10.3390/ma11020287.

23 L. Giraldo, A. Erto and J. C. Moreno-Piraján, *Adsorption*, 2012, **19**, 465–474.

24 H. S. Hassan, M. F. Elkady, E. E. Hafez and E. Salama, *Nanosci. Nanotechnol.–Asia*, 2017, **7**, 62–72.

25 X. H. Zhou, B. C. Huang, T. Zhou, Y. C. Liu and H. C. Shi, *Chemosphere*, 2015, **119**, 568–576.

26 S. A. Elfeky, S. E. Mahmoud and A. F. Youssef, *J. Adv. Res.*, 2017, **8**, 435–443.

27 M. O. Ojemaye, O. O. Okoh and A. I. Okoh, *Mater. Express*, 2017, **7**, 439–456.

28 A. Becker and K. Soliman, *Neurochem. Res.*, 2009, **34**, 1677–1684.

29 S. Lan, L. Liu, R. Li, Z. Leng and S. Gan, *Ind. Eng. Chem. Res.*, 2014, **53**, 3131–3139.

30 M. Fuji, Y. S. Han and C. Takai, *KONA Powder Part. J.*, 2013, **30**, 47–68.

31 X. Gao, H. B. Wu, L. Zheng, Y. Zhong, Y. Hu and X. W. Lou, *Angew. Chem., Int. Ed.*, 2014, **53**, 5917–5921.

32 Y. Wu, E. Hu, W. Dai, Z. Li, Y. Zhong and Y. Hu, *RSC Adv.*, 2017, **7**, 5093–5100.

33 L. Mao, J. Li, Y. Xie, Y. Zhong and Y. Hu, *RSC Adv.*, 2014, **4**, 29698–29701.

34 M. B. Gawande, S. N. Shelke, R. Zboril and R. S. Varma, *Acc. Chem. Res.*, 2014, **47**, 1338–1348.

35 Y. Cho, C. H. Shin and S. Han, *Nanoscale Res. Lett.*, 2016, **11**, 1–9.

36 P. Pfaffli, A. Zitting and H. Vainio, *Scand. J. Work, Environ. Health*, 1978, **4**, 22–27.

37 H. Noei, H. Qiu, Y. Wang, E. Loffler, C. Woll and M. Muhler, *Phys. Chem. Chem. Phys.*, 2008, **10**, 7092–7097.

38 A. Kumar, S. Arora, N. Mogha, S. S. Al-Deyab, Z. A. Ansari and S. G. Ansari, *Energy Environ. Focus*, 2013, **2**, 101–107.

39 P. P. Sharmila and N. J. Tharayil, *IOP Conf. Ser.: Mater. Sci. Eng.*, 2015, **73**, 012019.

40 H. Kumar and R. Rani, *Int. Lett. Chem., Phys. Astron.*, 2013, **14**, 26–36.

41 A. H. Moharram, S. A. Mansour, M. A. Hussein and M. Rashad, *J. Nanomater.*, 2014, **2014**, 1–5.

42 S. Liufu, H. Xiao and Y. Li, *Polym. Degrad. Stab.*, 2005, **87**, 103–110.

43 V. T. Bhugul and G. N. Choudhari, *International Journal of Scientific and Research Publications*, 2015, **5**(1), 2250–3153.

44 A. Marraa, C. Silvestrea, D. Duraccio and S. Cimminoa, *Int. J. Biol. Macromol.*, 2016, **88**, 254–262.

45 J. M. Berg, A. Romoser, N. Banarjee, R. Zebda and C. M. Sayes, *Nanotoxicology*, 2009, **3**, 276–283.

46 D. T. Tran, *RSC Adv.*, 2016, **6**, 1339–1345.

47 S. Ahad, A. Bashir, T. Manzoor and A. H. Pandith, *RSC Adv.*, 2016, **6**, 35914–35927.

48 A. Stafiej and K. Pyrzynska, *Sep. Purif. Technol.*, 2007, **58**, 49–52.

49 I. Langmuir, *J. Am. Chem. Soc.*, 1918, **40**, 1361–1403.

50 F. K. Onwu, C. U. Sonde and J. C. Igwe, *J. Phys. Chem.*, 2014, **3**, 89–95.

51 A. Farrukh, A. Akram, A. Ghaffar, S. Hanif, A. Hamid, H. Duran and B. Yameen, *ACS Appl. Mater. Interfaces*, 2013, **5**, 3784–3793.

52 M. Monier, *Int. J. Biol. Macromol.*, 2012, **50**, 773–781.

53 J. J. Alcaraz-Espinoza, A. E. Chávez-Guajardo, J. C. Medina-Llamas, C. A. S. Andrade and C. P. de Melo, *ACS Appl. Mater. Interfaces*, 2015, **7**, 7231–7240.

54 H. Nakayama, S. Hirami and M. Tsuhako, *J. Colloid Interface Sci.*, 2007, **315**, 177–183.

55 Y. Zhao, Y. Chen, M. Li, S. Zhou, A. Xue and W. Xing, *J. Hazard. Mater.*, 2009, **71**, 640–646.

56 Z. H. Fard, C. D. Malliakas, J. L. Mertz and M. G. Kanatzidis, *Chem. Mater.*, 2015, **27**, 1925–1928.

57 M. J. Manos and M. G. Kanatzidis, *Chem. - Eur. J.*, 2009, **15**, 4779–4784.

58 M. Naushad, Z. A. ALOthman, M. R. Awual, M. M. Alam and G. E. Eldesoky, *Ionics*, 2015, **21**, 2237–2245.

59 T. T. Liu, M. Yang, T. X. Wang and Q. P. Yuan, *Ind. Eng. Chem. Res.*, 2012, **51**, 454–463.

60 A. K. Bhattacharya, T. K. Naiya, S. N. Mandal and S. K. Das, *Chem. Eng. J.*, 2008, **137**, 529–541.